

# Analytical model of Europa's O<sub>2</sub> exosphere

---

Anna Milillo (anna.milillo@iaps.inaf.it), Christina Plainaki, Elisabetta De Angelis, Valeria Mangano, Stefano Massetti, Alessandro Mura, Stefano Orsini, Rosanna Rispoli

INAF/Istituto di Astrofisica e Planetologia Spaziali, via del Fosso del Cavaliere, 00133 Rome, Italy

## Abstract

The origin of the exosphere of Europa is its water ice surface. The existing exosphere models, assuming either a collisionless environment (simple Monte Carlo techniques) or a kinetic approach (Direct Monte Carlo Method) both predict that the major constituent of the exosphere is molecular oxygen. Specifically, O<sub>2</sub> is generated at the surface through radiolysis and chemical interactions of the water dissociation products. The non-escaping O<sub>2</sub> molecules circulate around the moon impacting the surface several times, due to their long lifetime and due to their non-sticking, suffering thermalization to the surface temperature after each impact. In fact, the HST observations of the O emission lines proved the presence of an asymmetric atomic Oxygen distribution, related to a thin asymmetric molecular Oxygen atmosphere. The existing Monte Carlo models are not easily applicable as input of simulations devoted to the study of the plasma interactions with the moon. On the other hand, the simple exponential density profiles cannot well depict the higher temperature/higher altitudes component originating by radiolysis. It would thus be important to have a suitable and user-friendly model able to describe the major exospheric characteristics to use as a tool.

This study presents an analytical 3D model that is able to describe the molecular Oxygen exosphere by reproducing the two-component profiles and the asymmetries due to diverse configurations among Europa, Jupiter and the Sun. This model is obtained by a non-linear fit procedure of the EGEON Monte Carlo model (Plainaki et al. 2013) to a Chamberlain density profile. Different parameters of the model are able to describe various exosphere properties thus allowing a detailed investigation of the exospheric characteristics. As an example a discussion on the exospheric temperatures in different configurations and space regions is given.

## 1 Introduction

Among the different bodies of our Solar System, the icy moons of Jupiter experience a strong interaction with the magnetospheric plasma; in fact, the Galileo mission data analysis showed that these moons are continuously irradiated by energetic ions (H<sup>+</sup>, O<sup>+</sup> and S<sup>+</sup>) and electrons in the energy range from keV to MeV (Cooper et al., 2001; Paranicas et al., 2002). Even if the details of the processes and their impact on the near-body environment are still to be investigated, there is agreement within the science community that the origin of the exosphere of Europa is its water ice surface. More specifically, the surface components (mainly water) in atomic or molecular form are released almost stoichiometrically via ion-sputtering (Johnson et al. 2009); while O<sub>2</sub> and H<sub>2</sub> molecules are released in the exosphere in a two-step process, i.e.

water dissociation via radiolysis ( $\text{OH} + \text{H}$ ) and chemical recombination which produce at the end molecular Oxygen and Hydrogen. The gas molecules are then released (Cassidy et al., 2010) and follow ballistic trajectories until they redeposit or bounce to the surface, or escape from the gravity field or are ionized and picked up.

Europa's  $\text{O}_2$  environment can be considered as a transitional case between a (collisional) atmosphere and a (collisionless) exosphere (Leblanc et al. 2002; Plainaki et al., 2010). Nonetheless the atmosphere is so tenuous that it does not act as a significant obstacle to escaping particles released from its surface. The existing exosphere models, assuming either a collisionless environment (simple Monte Carlo techniques) (e.g. Johnson et al., 2004; Cassidy et al., 2010; Plainaki et al., 2010; 2012; 2013) or a kinetic (Direct Monte Carlo Method) (Shematovich et al., 2005; Smyth and Marconi, 2006) or numerical (Saur et al. 1998) approach, all predict that the major constituent of the exosphere is molecular Oxygen. This is mainly due to two reasons: first, Oxygen does not freeze to the surface as water molecules do (Johnson et al., 1982, Shematovich et al., 2005) and second it lacks the sufficient energy to overcome Europa's gravity, contrary to  $\text{H}_2$  (Smyth and Marconi, 2006) that due to its low weight escapes from the moon much more easily. Even if, the  $\text{H}_2$  and  $\text{H}_2\text{O}$  components are expected to be the major constituents of the exosphere at higher altitudes (above about 500 km) (Plainaki et al. 2012; Smyth and Marconi, 2006), the  $\text{O}_2$  molecules are present in a relevant fraction up to high altitudes and the O-emission line (proxy of  $\text{O}_2$ ) is the only one presently observed.

Although direct observations of Europa's atmosphere do not yet exist, the presence of atmosphere asymmetries has been for long suspected, based on HST OI observations. Indeed observations of the 135.6 nm O-emission line (indicative of  $\text{O}_2$  dissociation) displayed spatially localized and asymmetric emissions (i.e.: McGrath et al., 2004, Saur et al., 2011). It has been assumed since then that asymmetric features could be attributed either to asymmetric e-populations impacting a homogeneous atmosphere or to a spatially non-uniform  $\text{O}_2$  atmosphere or both (see also discussion in Roth et al., 2014). Cassidy et al. (2007) hypothesized a non uniform  $\text{O}_2$  resulting from different local surface properties. Asymmetric emission of neutrals from Europa's surface was modeled for the first time by Plainaki et al. 2010, for all three main species (i.e.  $\text{H}_2\text{O}$ ,  $\text{O}_2$ ,  $\text{H}_2$ ). In that paper this asymmetric surface emission was attributed to different agents:

- a) to different sputtering efficiencies determined mainly by the spatial distribution of the energetic ion flux impacting the moon (i.e. the impacting ion flux becomes maximum at the trailing hemisphere apex) (more effective for the released  $\text{H}_2\text{O}$  population).
- b) to surface temperature distribution (peaking at the subsolar point) determining the efficiency of the radiolysis process, (producing asymmetries in the  $\text{O}_2$  and  $\text{H}_2$  populations mainly at higher altitudes).

In subsequent papers the  $\text{O}_2$  asymmetric emissions from the surface were further modeled (e.g. using more accurate yield functions (Plainaki et al., 2012) and studied for different orbital phases (Plainaki et al., 2013).

The outputs of the existing exosphere Monte Carlo models are not always easily applicable and/or integrated (for example, being used as inputs) in simulations devoted to the study of the plasma interactions with the moon. On the other hand, the simple exponential density profiles cannot well depict the higher temperature/higher altitudes component originating from the radiolytic release. It would thus be important to have a suitable and user-friendly model able to describe the major exospheric characteristics through a series of parameters related to the actual physical

mechanisms taking place and to the resulting spatial distribution of the neutral population.

This study presents an analytical 3D model that is able to describe the molecular Oxygen exosphere along the Europa orbit around Jupiter (forth dimension) by reproducing the asymmetries due to the variable configurations among Europa, Jupiter and the Sun, that is, the illumination phase angle and the two-components profile. This model is obtained by a non-linear fit procedure of the EGEON Monte Carlo model (Plainaki et al., 2013, referred as P2013 from here below) to a Chamberlain density profile.

The model development is described in Section 2 in relation to vertical profile (1D), equatorial distribution (2D), latitudinal distribution (3D) for the four configurations described by P2013 and in relation to orbit phase (4D). This first analysis is performed only for modelling the O<sub>2</sub> generated after the O<sup>+</sup> impact onto the surface. Discussion on correction factors and final description of the O<sub>2</sub> exosphere generated by all the major impacting ions is given in Section 2.7. In Section 3, we discuss the exospheric scale heights and temperatures trends derived by the model. A brief summary of the global model and conclusions are drawn in Section 4.

## 2 Model development

P2013 described the O<sub>2</sub> exosphere generated by different ions impacting the Europa surface in four Europa-Jupiter-Sun configurations by using the EGEON model runs of about 1M of particles for each configuration. The major loss process, i.e. electron impact dissociation is included in the EGEON model. A sketch of the four exospheric distributions in the equatorial plane along the orbit around Jupiter is given in Figure 1. The longitude definition is: 0° corresponds to Jupiter direction, 90° is the leading side, 180° anti-Jupiter, 270° trailing side. The Sun direction is in the equatorial plane and it is at longitude  $\alpha_S=90^\circ$  for Conf *a*,  $\alpha_S=180^\circ$  for Conf *d*,  $\alpha_S=270^\circ$  for Conf *c*,  $\alpha_S=0^\circ$  for Conf *b*.

We start to consider the Conf *a* generated after the O<sup>+</sup> impact where leading hemisphere corresponds to the illuminated side ( $\alpha_S=90^\circ$ ) and +x space, and Jupiter-facing hemisphere corresponds to +y space. We analyse the radial vertical profiles in the range  $R=1.05 - 5 R_E$  by fitting them with a Chamberlain function (Chamberlain, 1963):

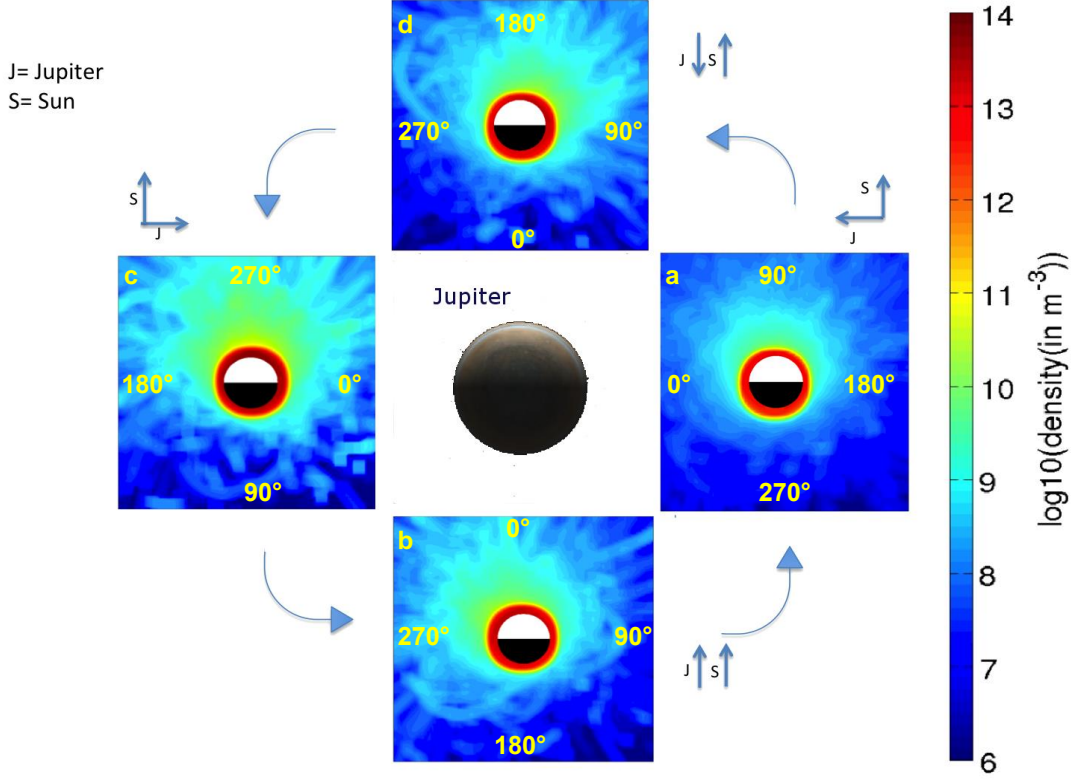


Figure 1 Monte Carlo simulated Europa's equatorial exosphere of  $O_2$  generated after  $O^+$  impacts in four configurations around Jupiter (from P2013). J vector indicates the Jupiter direction, S vector indicates the Sun direction. Longitudes are indicated in each panel together with the configuration as labelled in P2013.

$$\log_{10}\rho = d e^{-c(R-1)} - \frac{R-1}{a} + b, \quad (1)$$

where  $\rho$  is the density,  $R$  is the Europa centric distance (in Europa's radii) ranging between 1.05 and 5  $R_E$ , and,  $a$ ,  $b$ ,  $c$ ,  $d$  are free parameters. The  $a$  and  $b$  parameters, mostly describes the gradual high altitudes profile, while the parameters  $c$  and  $d$  mostly describes the low altitudes steeply density decrease. The parameters  $a$  and  $c$  describe the gradient of the radial profile ( $\rho'(R=1)=-1/a-dc$ ;  $\rho'(R\rightarrow\infty)=-1/a$ ), while  $b$  and  $d$  describe the absolute value of the density at high and low altitudes, respectively ( $\rho(R=1)=10^{b+d}$ ;  $\rho(R\rightarrow\infty)=10^b$ ).

To obtain the longitude,  $Ln$ , and latitude,  $Lt$ , dependence of the four parameters we perform an iterative process. We fit the vertical profile of the Monte Carlo simulated exosphere at different longitudes at latitude  $0^\circ$ , then we determine the functional form able to describe the four parameters ( $a(Ln)$ ,  $b(Ln)$ ,  $c(Ln)$ ,  $d(Ln)$ ). When the functional forms versus longitude are defined, we assume symmetry with respect to the subsolar point, angle  $\alpha$ , for configurations Conf  $a$  and Conf  $c$  and symmetry with respect a longitudinal-shifted angle for Conf  $b$  and Conf  $d$ . Then we fit different latitudes verifying that the functional form is valid and optimizing the parameter values.

At the end, the parameters are defined as a function of longitude and latitude, hence, a 3D function describing the global exosphere in each specific configuration is obtained.

Finally, we describe also the modulation of the parameters along the moon orbit.

As a final step, we apply a correction in the density taking into account the contribution of different impacting ions.

## 2.1 Conf-a: 1D analysis

The equatorial vertical profile of Conf *a* have been analysed to verify that the selected Chamberlain function well describes the density vs *r*.

Examples of fits at different longitudes at *Lt*=0 are shown in Figure 2. The fits have regression coefficients  $r^2 > 0.95$ .

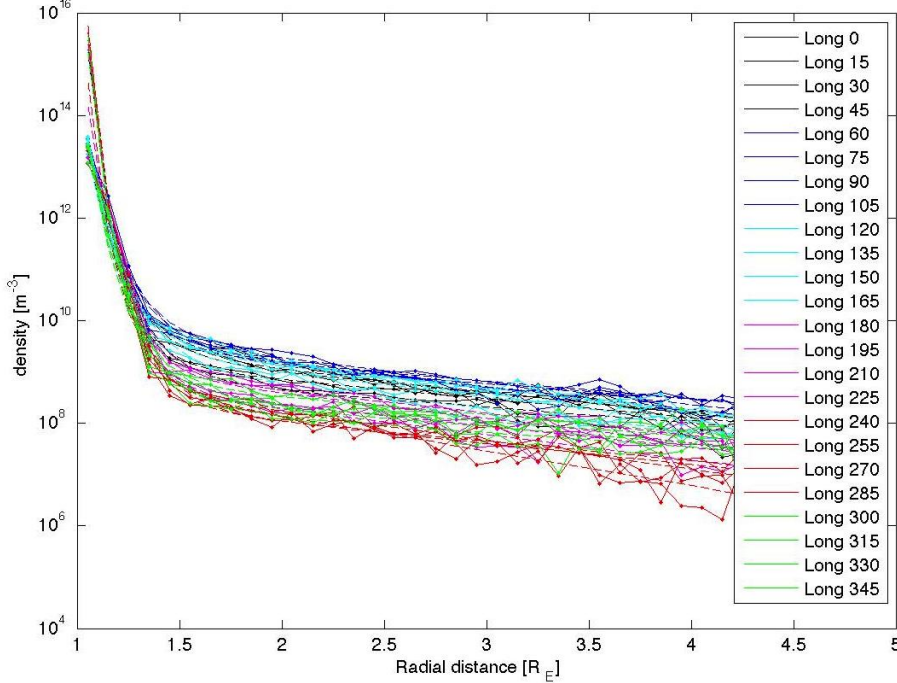


Figure 2 O<sub>2</sub> density profiles of Conf *a* for different longitudes at *Lt*=0°. Here the longitudes are considered at an interval of 15°. Points connected by solid lines are from the EGEON model results, and dashed lines are from the fit for each profile identified by colour as in the legend.

## 2.2 Conf-a: 2D analysis

The parameters as a function of longitude are plotted in Figure 3, together with the fit with the function  $F = pa + pb \sin(Ln)$ . Parameter *a* and *c* seem to have no trend vs longitude, in fact the regression coefficient  $r^2$  is  $< 0.6$  (not shown), while parameters *b* and *d* are described by the fit function. Generally, in this study, we assume that the functions are not representative of the trends when  $r^2 < 0.6$ . Results of these fits are listed in Table 1, where the “value” is the weighted average of the parameters with the standard deviation and “relative error” is the ratio between these two quantities:

$$\bar{p} = \frac{\sum p_i 1/\Delta p_i}{\sum 1/\Delta p_i} \quad (2)$$

$$\Delta \bar{p} = \sqrt{\frac{1}{(\sum 1/\Delta p_i - 1)} \sum \left[ 1/\Delta p_i (p_i - \bar{p})^2 \right]}$$

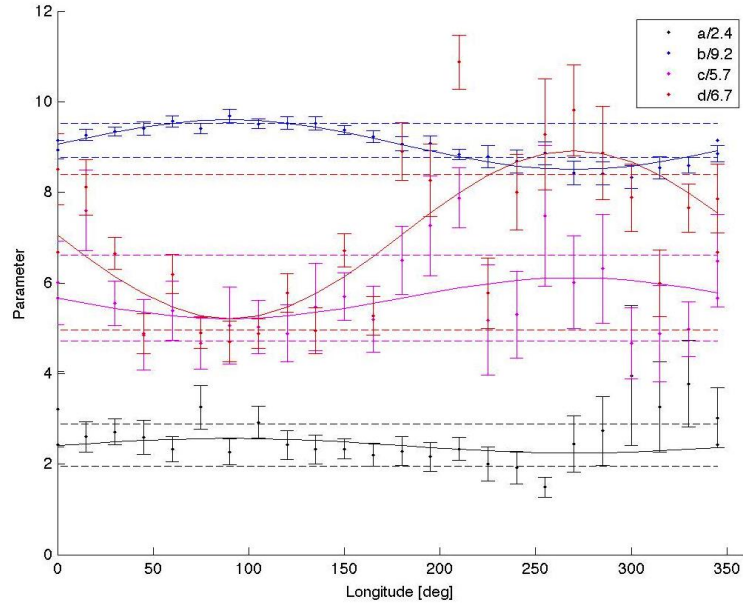


Figure 3. Conf *a* parameters *a*, *b*, *c* and *d* vs *Ln*. Confidence intervals are shown with dashed lines and fits are shown with solid lines.

Table 1 Results of 4- parameters analysis with function  $pa+pb*\sin(Ln)$

Parameter	Average	Relative error	pa	pb	r <sup>2</sup>
<b>a</b>	2.4±0.5	0.2	-	-	-
<b>b</b>	9.2±0.4	0.04	9.07±0.06	0.56±0.08	0.897
<b>c</b>	5.7±0.9	0.15	-	-	-
<b>d</b>	6.7±2	0.3	7.24±0.5	-2.3±0.7	0.643

Finally, the adopted functional forms of the parameters are listed in Table 2.

Table 2 Results of *a*, *b*, *c* and *d* functional forms versus *Ln*

Parameter	function
<i>a</i>	p1
<i>b</i>	p2+p3*sin( <i>Ln</i> )
<i>c</i>	p4
<i>d</i>	p5+p6*sin( <i>Ln</i> )

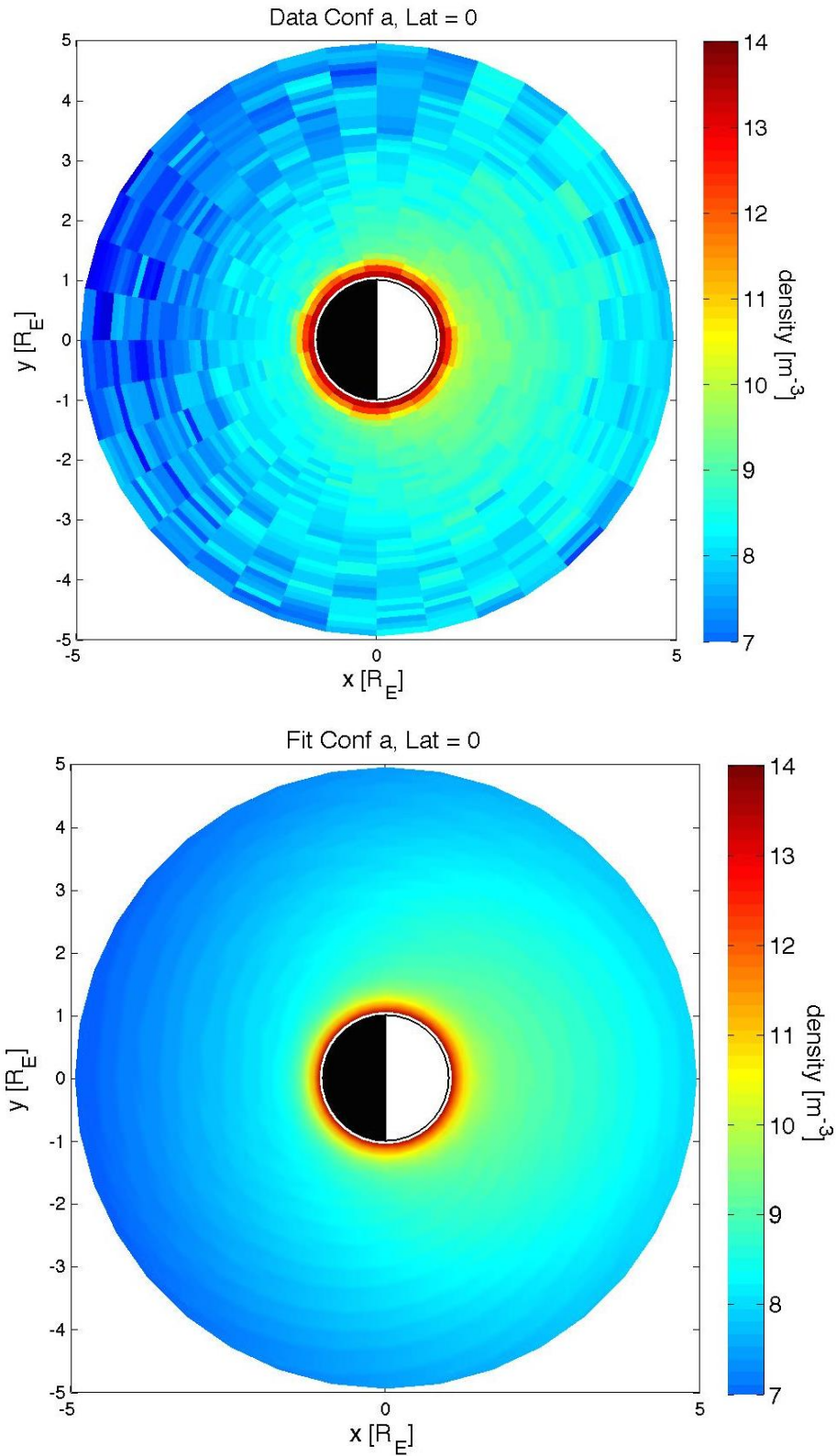


Figure 4 Above: Monte Carlo simulated equatorial exosphere of  $\text{O}_2$  generated after  $\text{O}^+$  impacts in the configuration *a* of P2013: leading corresponding to the illuminated side +x direction, Jupiter facing hemisphere in +y direction. Below: density ( $\text{O}_2$  after  $\text{O}^+$ ) obtained by 2D fit in the equatorial plane

The density at latitude  $0^\circ$  as a function of radial distance ( $R$ ) and longitude ( $Ln$ ) is shown in Figure 4 and described by the following function:

$$\log_{10}\rho (R, Ln, Lt = 0) = (p5 + p6 \sin(Ln)) e^{-(p4)(R-1)} - \frac{(R-1)}{p1} + p2 + p3 \sin(Ln) \quad (3)$$

### 2.3 Conf-a: 3D analysis

The dependence on the angle from the Sun zenith direction,  $\alpha$ , in the equatorial plane is  $\alpha_{eq} = Ln - \alpha_s$ , and in off equatorial plane is  $\alpha_{lt} = Lt$ .

Considering a cylindrical symmetry of the distribution in respect to the Sun direction, we can extend the function (3) in the third dimension by substituting the  $\sin(Ln)$  dependence with the cosine of the subsolar angle,  $\alpha$ .

$$\cos(\alpha) = \cos(\alpha_{eq})\cos(\alpha_{lt}) = \cos(Ln - \alpha_s) \cos(Lt) \quad (4)$$

so that the final function becomes:

$$\log_{10}\rho (R, \alpha) = (p5 + p6 \cos(\alpha)) e^{-(p4)(R-1)} - \frac{(R-1)}{p1} + p2 + p3 \cos(\alpha) \quad (5)$$

This function has been applied to obtain a 2D best fit with six free parameters of the density at different latitudes at radial distances  $R$  between 1.05 and 5  $R_E$ . The 2D fit has been performed for each latitude (interval of  $10^\circ$ ), so that finally a 3D description can be derived. The fits have regression coefficients  $r^2 > 0.945$ .

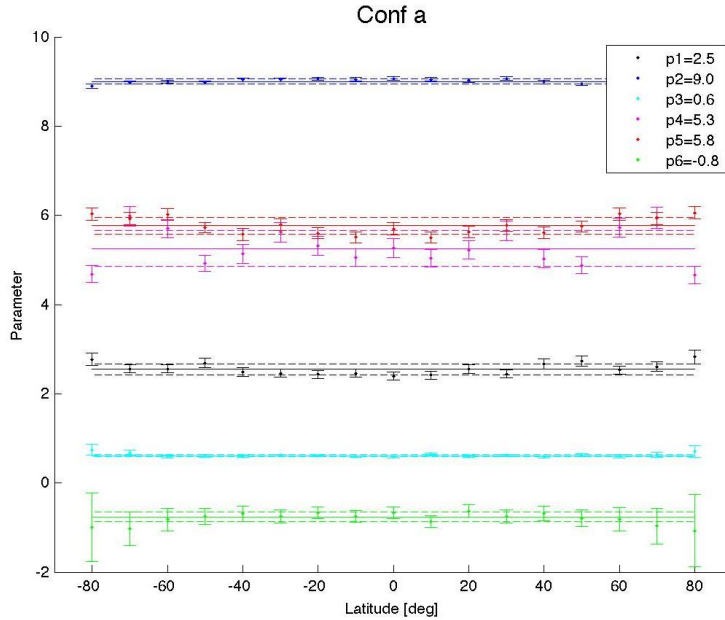


Figure 5 6-parameter fit Parameters vs  $Lt$  for Conf a. Weighted averages and errors are indicated by solid and dashed lines.

The final parameters, resulting from the fit procedure are shown in Figure 5 and listed in Table 3. The absence of a trend in the plots of Figure 5 is an indication that the adopted trend vs  $Lt$  is correct.

Table 3 Results of parameters analysis case O<sup>+</sup> Conf a

Parameter	Value	Rel. err.
p1	2.54(±0.1)	0.04
p2	9.00(±0.05)	0.007
p3	0.61(±0.03)	0.05
p4	5.25(±0.3)	0.06
p5	5.77(±0.2)	0.03
p6	-0.76(±0.06)	0.08

## 2.4 Case Conf-c

In the case of  $O_2$  released after  $O^+$  impact when the trailing side is illuminated by the Sun,  $\alpha_S = 270^\circ$  (Conf *c*), the same functional form of Conf *a* has been adopted. The 2D best fits with six free parameters of the density at different latitudes at radial distances  $R$  between 1.05 and 5  $R_E$  have been performed. In Figure 6 the resulting fit in the equatorial plane is shown. The resulting parameters for Conf *c* versus  $Lt$  are plotted in Figure 7 and listed in Table 4.

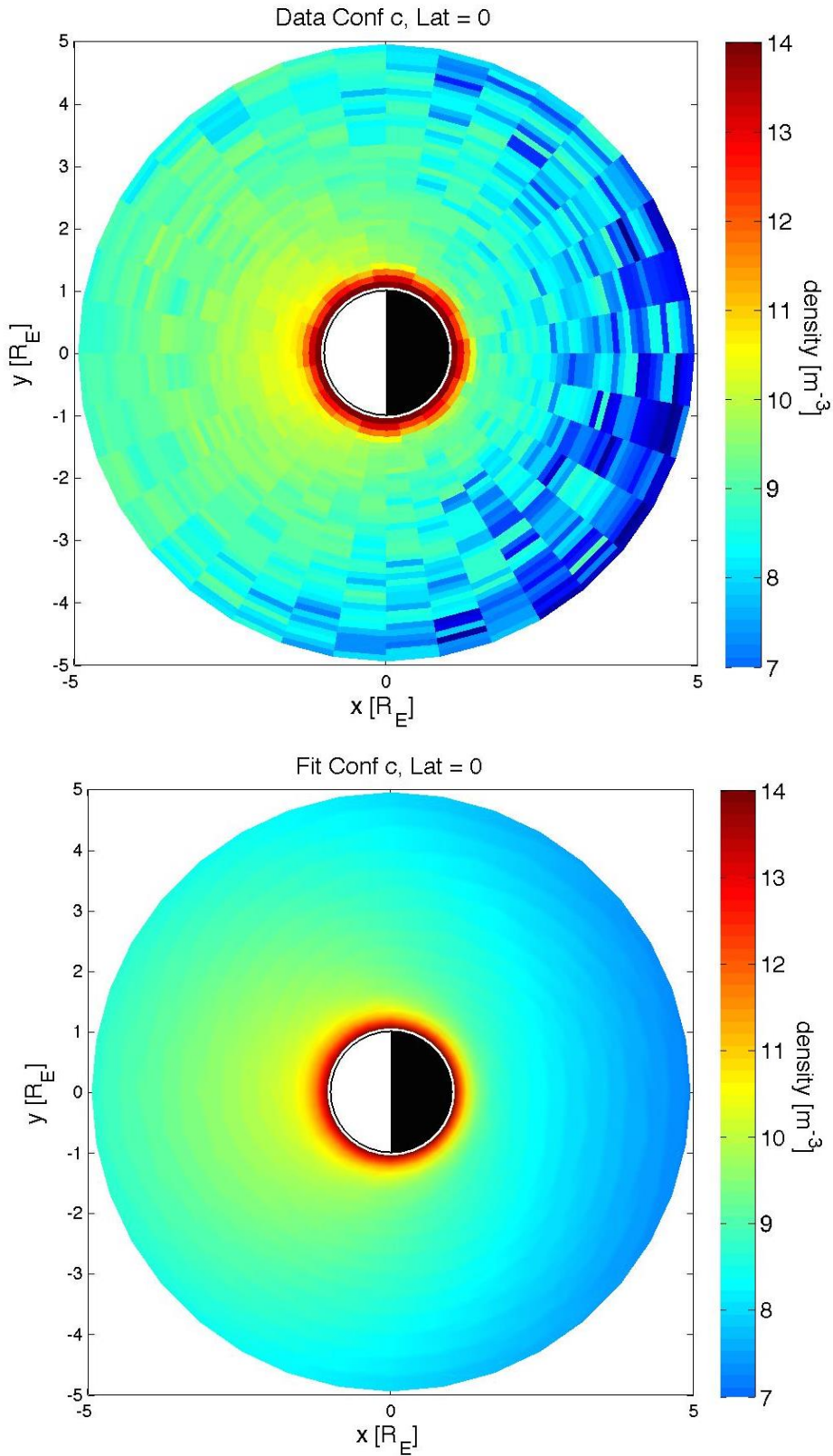


Figure 6 Same as Figure 4 for Conf *c*. Above: Monte Carlo simulated equatorial exosphere of  $\text{O}_2$  generated after  $\text{O}^+$  impacts in the configuration *c* of P2013. Below: density ( $\text{O}_2$  after  $\text{O}^+$ ) obtained by 2D fit in the equatorial plane

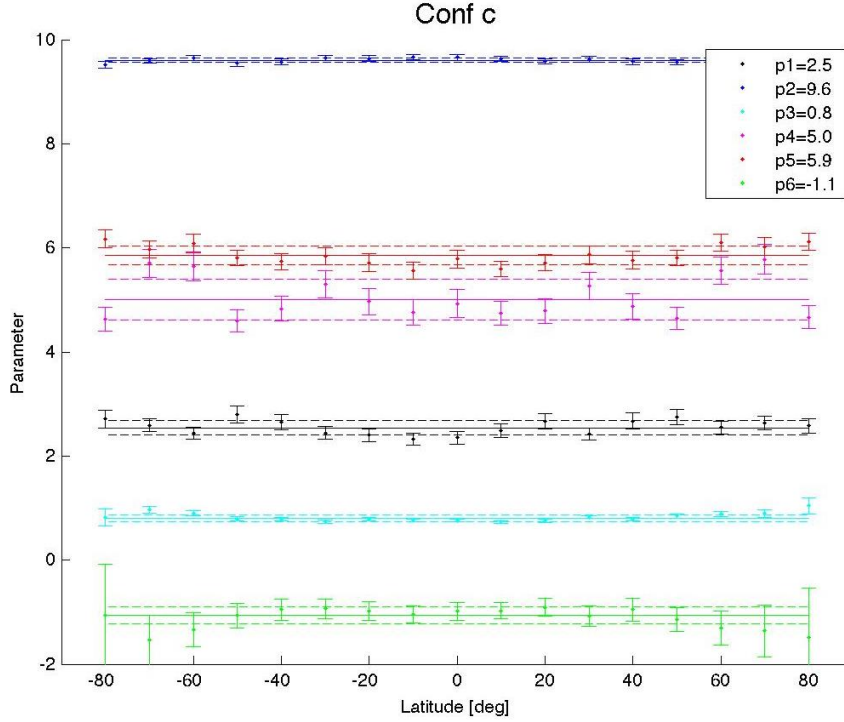


Figure 7 Same as Figure 5. Parameters vs  $Lt$  for Conf  $c$ .

Table 4 Results of parameters analysis case  $O^+$  Conf  $c$

Parameter	Value	Rel. err.
<b>p1</b>	<b>2.54(±0.1)</b>	0.04
<b>p2</b>	<b>9.60(±0.04)</b>	0.004
<b>p3</b>	<b>0.80(±0.06)</b>	0.08
<b>p4</b>	<b>5.0(±0.3)</b>	0.06
<b>p5</b>	<b>5.86(±0.2)</b>	0.03
<b>p6</b>	<b>-1.07(±0.06)</b>	0.06

We can note that the density in this configuration is higher than the configuration  $a$  as well described by the parameter  $p2$ .

## 2.5 Cases Conf- $b$ and Conf- $d$

In the case of  $O_2$  released after  $O^+$  impact when the Sun is toward Jupiter or anti Jupiter (Figure 1), the density has a maximum at an angle between the subsolar point and the trailing direction. We need to use a new parameter to describe the shift angle. To be sure that a simple shift describes these configurations, we performed the 1D fit with eq. (1) and analysed the 4 free parameters of the density profiles versus  $Ln$  in the equatorial plane at radial distances  $R$  between 1.05 and 5  $R_E$ . The fits are shown in Figure 8 and the parameters as a function of longitude are plotted in Figure 9 together with the fit with the function  $F = pa + pb \cos(Ln+pc)$ . The 4-parameters analyses are listed in Table 5 and Table 6.

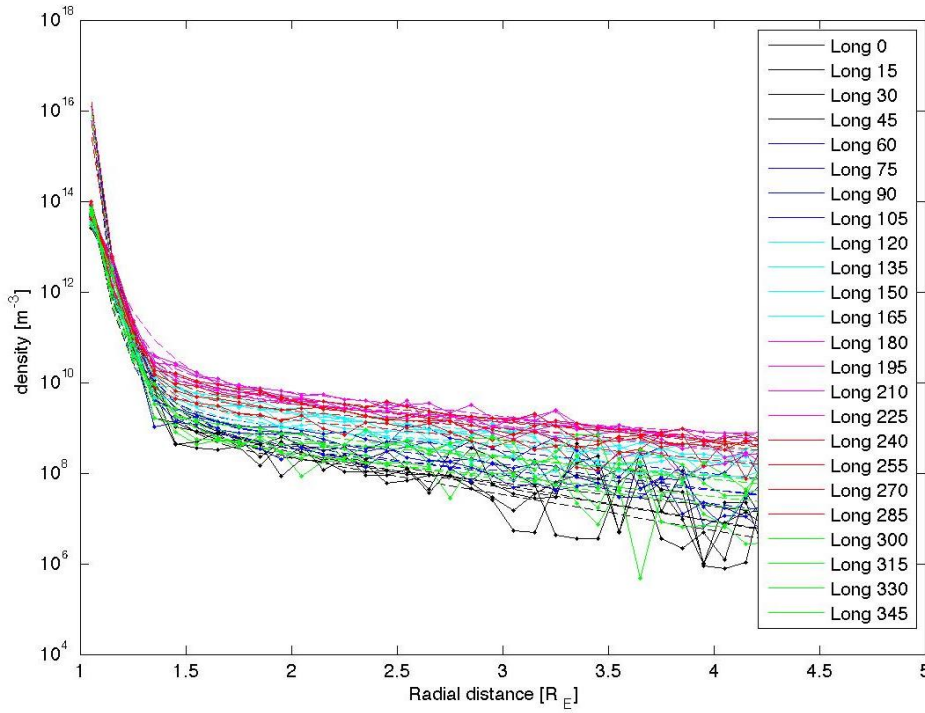
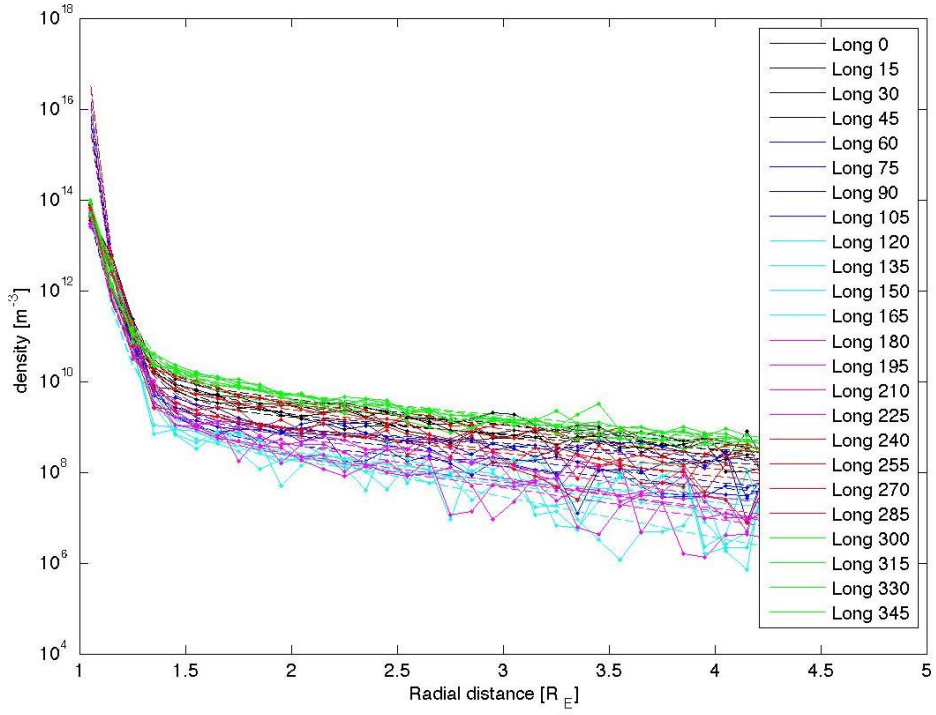


Figure 8. As in Figure 2. 4-parameters fit of density profile Conf b (above) and Conf d (below) for all longitudes.

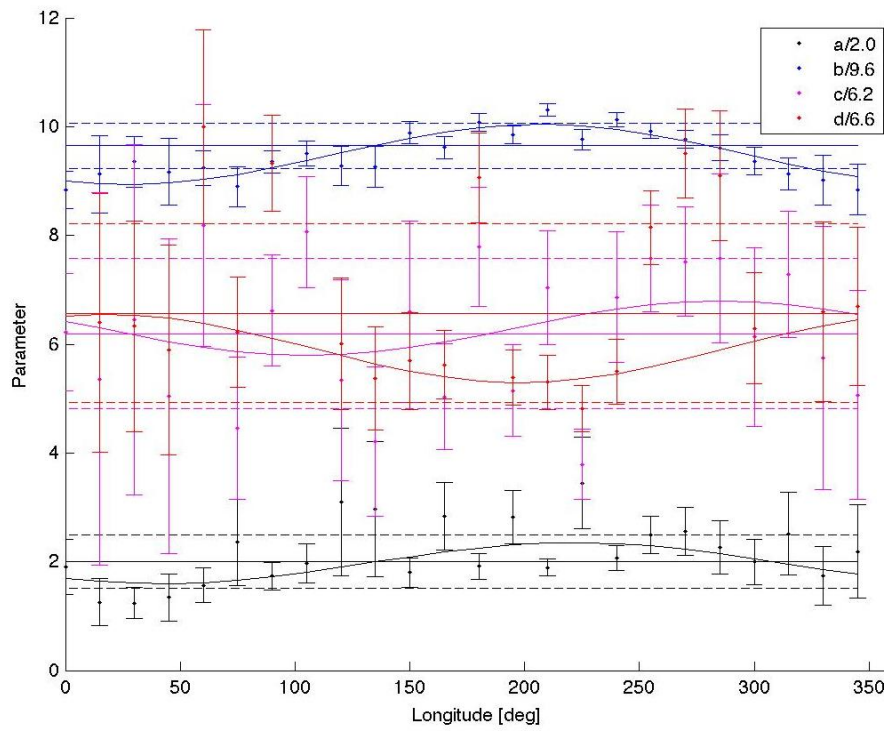
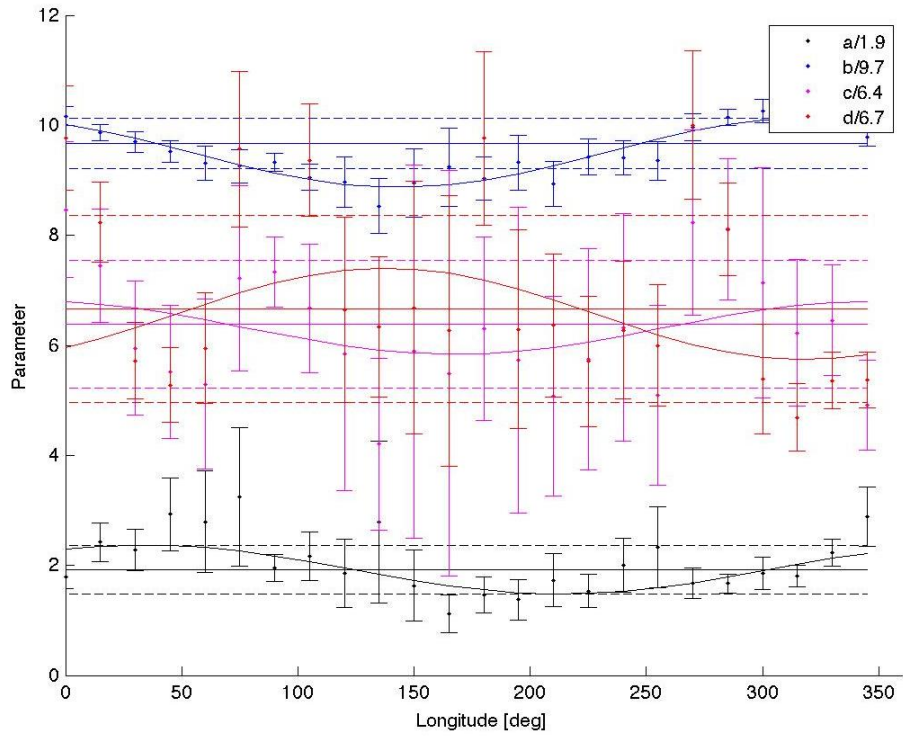


Figure 9. Conf b and Conf d parameters  $a, b, c$  and  $d$  vs  $Ln$  and weighted average intervals, fit function  $F=pa + pb \cos(Ln+pc)$  is indicated by solid lines.

Table 5 Results of 4- parameters analysis for Conf b with function  $pa+pb*\cos(Ln+pc)$

Parameter	Average	Relative error	pa	pb	pc	r <sup>2</sup>
a	1.9±0.4	0.21	-	-	-	-
b	9.665±0.4	0.4	9.51±0.09	0.64±0.1	-37±10	0.857
c	6.4±1	0.16	-	-	-	-
d	6.7±2	0.3	-	-	-	-

**Table 6 Results of 4- parameters analysis for Conf d with function  $pa+pb*\cos(Ln+pc)$**

Parameter	Average	Relative error	pa	pb	pc	r <sup>2</sup>
<b>a</b>	2.0±0.5	0.25	-	-	-	-
<b>b</b>	9.65±0.4	0.4	9.5±0.1	-0.55±0.1	27±15	0.742
<b>c</b>	6.2±1	0.16	-	-	-	-
<b>d</b>	6.6±2	0.3	5.9±0.5	-0.6±0.7	20±60	0.713

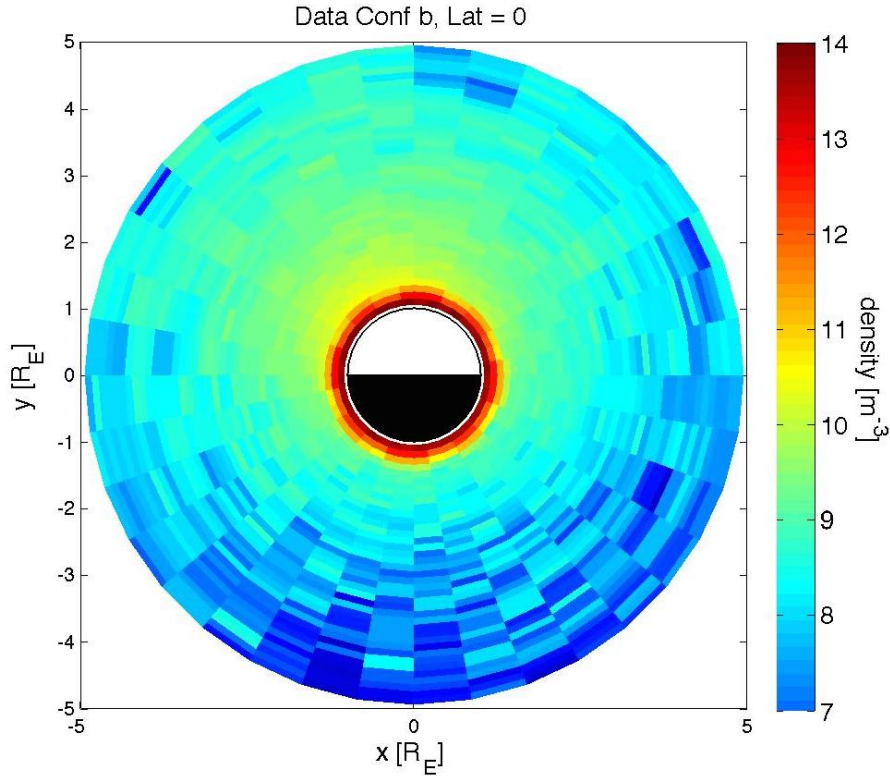
Parameter b has again a clear trend versus Ln and an offset of  $-37^\circ$  for Conf b, the same parameter for Conf d has a shifted trend (following the subsolar longitude  $\alpha_S = 180^\circ$ ), in fact the pb sign is opposite for the two configurations with an offset of  $+27^\circ$ . Parameter d seems to have a trend only for Conf d. The other parameters have no clear trend vs longitude as in the other configurations. For coherence with the previous functional form (5), we consider the function:

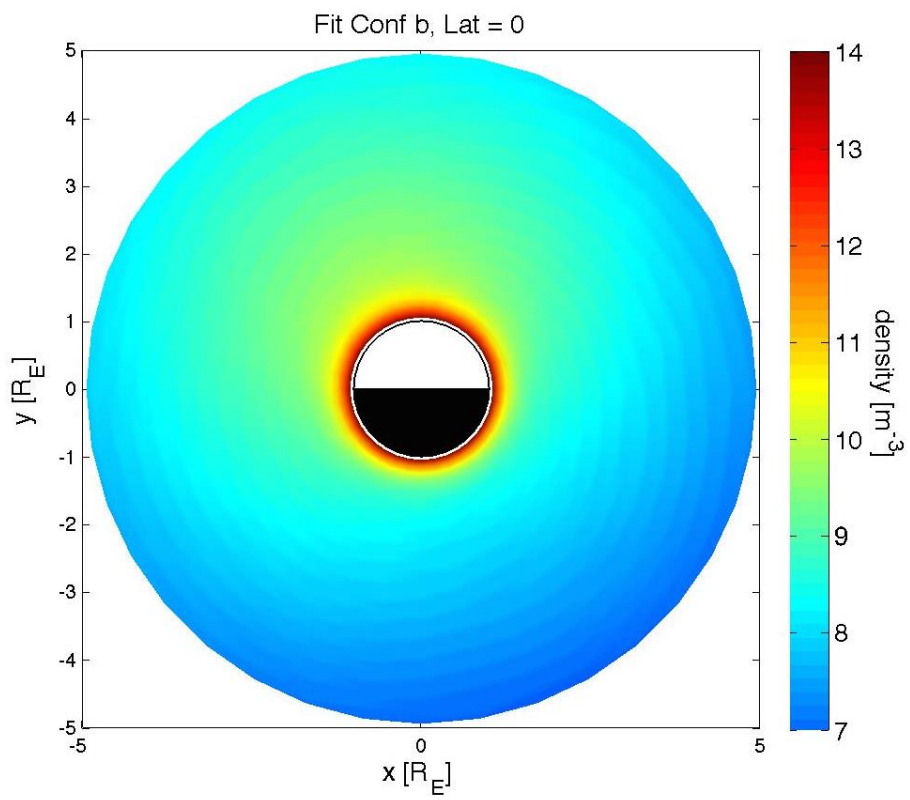
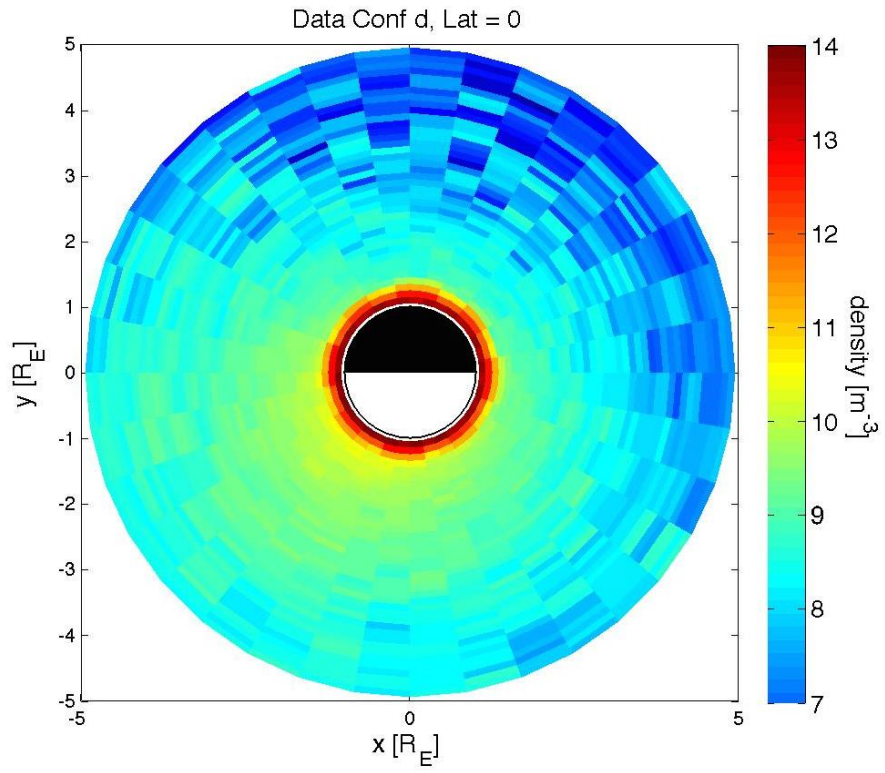
$$\log_{10}\rho(R, \alpha_{eq}, \alpha_{lt}) = (p5 + p6\cos(\alpha_{eq} - p7)\cos(\alpha_{lt})) e^{-(p4)(R-1)} - \frac{(R-1)}{p1} + p2 + p3\cos(\alpha_{eq} - p7)\cos(\alpha_{lt}) \quad (6)$$

where p7 is an angle function of the  $\alpha_S$ , it is null at  $\alpha_S=90^\circ$  and  $270^\circ$  and maximum/minimum at  $\alpha_S=0^\circ / 180^\circ$ . For simplicity we consider the same p7 parameter for low and high altitudes. Finally, the functional forms of the parameters a, b, c, and d, as a function of the Sun-zenith angle,  $\alpha$ , are listed in Table 7.

**Table 7 Results of a, b, c and d functional forms versus  $\alpha$**

Parameter	function
<b>a</b>	p1
<b>b</b>	p2+p3*cos( $\alpha$ -p7)
<b>c</b>	p4
<b>d</b>	p5+p6*cos( $\alpha$ -p7)





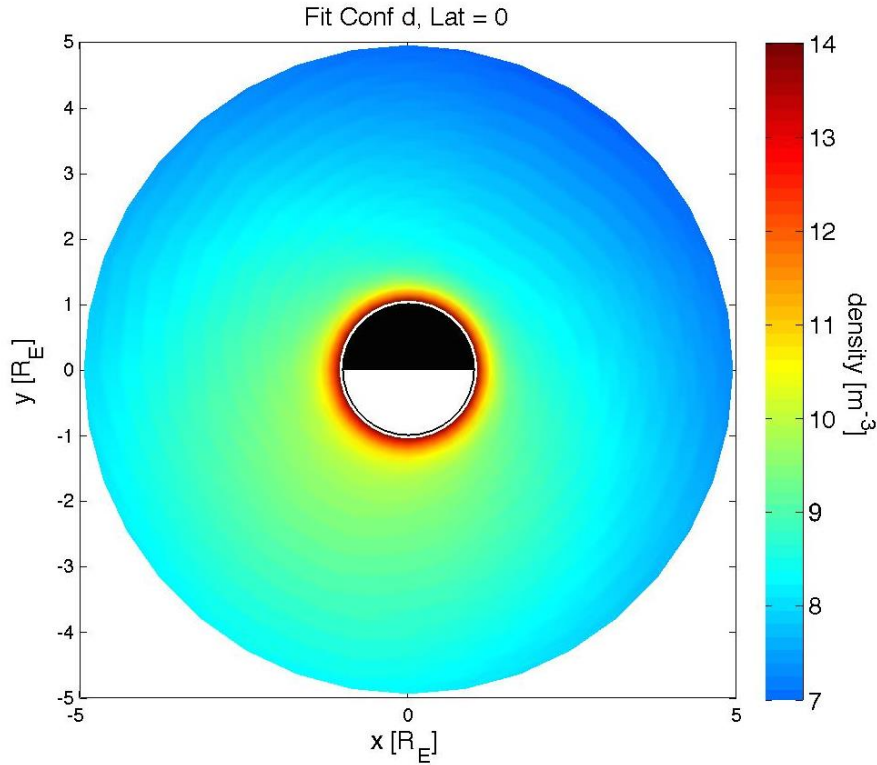
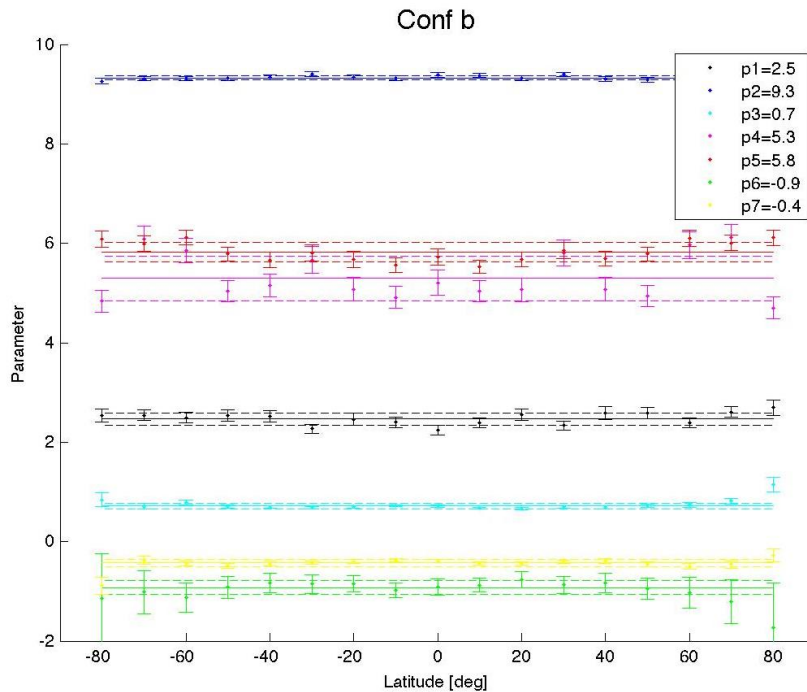


Figure 10 Same of Figure 4 for Conf *b* and Conf *d*. From above: P2013 Monte Carlo simulated equatorial exosphere of O<sub>2</sub> generated after O<sup>+</sup> impacts in Conf *b*; in Conf *d*; density obtained by 2D fit in the equatorial plane for Conf *b*; for Conf *d*;

Repeating the same procedure of Conf *a* and Conf *c* for these other configurations the resulting fits at the equatorial plane are shown in Figure 10. The resulting parameters versus *Lt* are plotted in Figure 11 and listed in Table 8



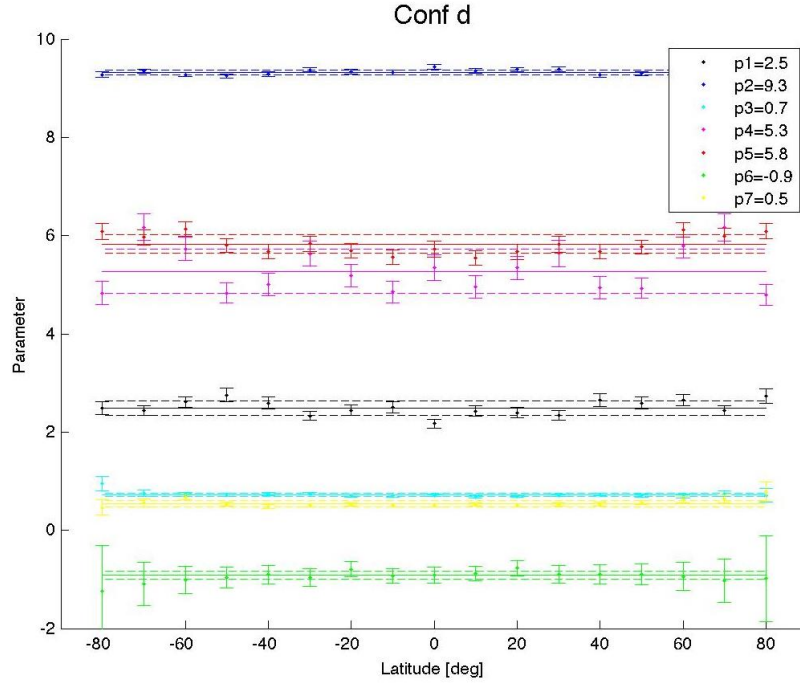


Figure 11 Same as Figure 5. Parameters vs Lt for Conf *b* above and Conf *d* below. Parameter *p7* is expressed in radians.

Table 8 Results of parameters analysis case O<sup>+</sup> Conf *b* and Conf *d*

Parameter	Value (Conf <i>b</i> )	Rel. err. (Conf <i>b</i> )	Value(Conf <i>d</i> )	Rel. err. (Conf <i>d</i> )
<b>p1</b>	<b>2.47(±0.1)</b>	0.04	<b>2.48(±0.2)</b>	0.08
<b>p2</b>	<b>9.33(±0.05)</b>	0.005	<b>9.32(±0.05)</b>	0.005
<b>p3</b>	<b>0.71(±0.06)</b>	0.08	<b>0.72(±0.03)</b>	0.04
<b>p4</b>	<b>5.29(±0.5)</b>	0.09	<b>5.27(±0.5)</b>	0.09
<b>p5</b>	<b>5.83(±0.2)</b>	0.03	<b>5.83(±0.08)</b>	0.01
<b>p6</b>	<b>-0.92(±0.1)</b>	0.1	<b>-0.91(±0.06)</b>	0.07
<b>p7</b>	<b>-25(±4)</b>	0.2	<b>31(±3)</b>	0.1

## 2.6 Dependence by orbit phase

From the resulting fit parameters it is clear that some of them modulate along the Europa orbit around Jupiter while others are about constant.

We consider as constant parameters (values within the error in the four configurations) *p1* and *p4*, which are the parameters describing the profile versus altitude.

We express the parameters *p2*, *p3*, *p5*, *p6* and *p7* as a function of orbit phase, that is, of the position of the Sun,  $\alpha_s$ . Having only four points, we suggest a simple harmonic function; hence, the functional forms of each parameters are expressed in Table 9.

Finally a 4D analytical model is obtained.

Table 9. Functional form of the parameters

Parameter	Functional forms	Functions
<b>p1</b>	const	2.51
<b>p2</b>	$p2(\alpha_s=0)-(p2(\alpha_s=270)-p2(\alpha_s=90))/2*\sin(\alpha_s)$	$9.3-0.3*\sin(\alpha_s)$
<b>p3</b>	$p3(\alpha_s=0)-(p3(\alpha_s=270)-p3(\alpha_s=90))/2*\sin(\alpha_s)$	$0.71-0.09*\sin(\alpha_s)$
<b>p4</b>	const	5.2
<b>p5</b>	$p5(\alpha_s=0)-(p5(\alpha_s=270)-p5(\alpha_s=90))/2*\sin(\alpha_s)$	$5.825-0.045*\sin(\alpha_s)$
<b>p6</b>	$p6(\alpha_s=0)-(p6(\alpha_s=270)-p6(\alpha_s=90))/2*\sin(\alpha_s)$	$-0.92+0.155*\sin(\alpha_s)$

$p^7$	$p^7(\alpha_s=0) * \cos(\alpha_s)$	$-28 * \cos(\alpha_s)$
-------	------------------------------------	------------------------

## 2.7 Corrections

To obtain the total O<sub>2</sub> density at Europa, the obtained parameters must be corrected for two reasons.

- 1) The O<sub>2</sub> release yields used in P2013 need to be revised similarly to the updates in Plainaki et al. (2015) following the argumentations described in Section 2.7.1.
- 2) This analysis has been performed by considering only the O<sup>+</sup> ions impacting the icy surface. The contribution of different ions, mainly H<sup>+</sup> and S<sup>+</sup> must be added to this density profile according to the argumentations described in Section 2.7.2.

### 2.7.1 Yield revision

In P2013 an erroneous interpretation of the surface-binding energy parameter,  $U$ , included in the Famà et al. (2008) formula had been considered. In particular, while incorporating the Famà formula in the EGEON model, the experimentally derived value of  $U = 0.05$  eV (Boring et al., 1984; Brown et al., 1984) was considered. However, such a consideration ignored the fact that the original lab data were fit in a formula that used the value of the water sublimation energy,  $U = 0.45$  eV, rather than the experimentally derived value. Therefore, the yield values, in the whole energy range and for all three species (H<sup>+</sup>, O<sup>+</sup>, S<sup>+</sup>), must be corrected by a factor  $c_1$ , equal to  $0.05/0.45$ .

Moreover, while calculating the O<sub>2</sub> release yield, within the EGEON model, only normal ion incidence had been considered. Whereas, non-normal ion incidence can increase the surface release yield (e.g. Johnson, 1990), the existence of regolith regions can lower the yield (Cassidy et al., 2013). The two effects on the yield could cancel each other. By considering the case of a pure ice surface, we choose to correct our calculations for the O<sub>2</sub> release yield by inserting an additional correction factor,  $c_2$ , that represents the angle-averaged yield. This factor is equal to the average value of  $\cos^f(\theta)$ , with the incidence angle  $\theta$  varying in the (0-70) degrees range (Wei et al., 2009). Therefore, for the incidence-angle correction factor,  $c_2$ , we derive the following values:

O<sup>+</sup> ( $m_1=16 \rightarrow f=1.7$ ):  $c_2=2$

S<sup>+</sup> ( $m_1=32 \rightarrow f=1.8$ ):  $c_2=2$

H<sup>+</sup> ( $m_1=1 \rightarrow f=1.3$ ):  $c_2=1.6$

A third correction to the formula of the yield regarding the fractioning of the Famà et al., (2008) formula must be considered. P2013 fractioned the temperature-dependent part of the formula,  $Y_{\text{diss}}(T)$ , in a stoichiometric way, that is, 2-to-1 H<sub>2</sub>-to-O<sub>2</sub> partitioning and, therefore,  $Y_{\text{O}_2}=1/3 * Y_{\text{diss}}(T)$  However, the mass of these molecules must be considered. This means that it is more correct to consider

$$Y_{\text{O}_2} = [m_{\text{H}_2\text{O}} / (m_{\text{O}_2} + 2m_{\text{H}_2})] \times Y_{\text{diss}}(E_i, T) = 1/2 Y_{\text{diss}}(E_i, T) = T_{\text{tot}}$$

Finally, this yield a third correction factor to be applied which is  $c_3=3/2$ .

In conclusion, the EGEON model of P2013 must be scaled by a factor of  $c_1 * c_2 * c_3 = 1/3$ , that is, a factor  $-\log_{10}(3)$  in function (6). This factor modifies only the  $p_2$  parameter.

### 2.7.2 Other ions effects

This analysis has been performed by considering only the O<sup>+</sup> impacting the icy surface. The contribution of different ions, i.e.: H<sup>+</sup> and S<sup>+</sup> must be added to this density profile. We can consider that H<sup>+</sup> and S<sup>+</sup> have similar impacting distributions,

so that the obtained released densities can be simply added to that obtained from O<sup>+</sup> impact to have the total O<sub>2</sub> density.

As summarized in Table 1 of P2013 the ratios of the density due to H<sup>+</sup> and to S<sup>+</sup> to the density due to O<sup>+</sup> are a factor 0.5 and 0.008, respectively.

To obtain the total O<sub>2</sub> density, the density after O<sup>+</sup> impact must be multiplied by a factor  $c_4 = 1.508$ , that is, a factor  $\log_{10}(1.508)$  in function (6). Also this factor modifies the parameter  $p_2$ , that finally becomes  $p_2 = p_2 - \log_{10}(3) + \log_{10}(1.508) = p_2 - 0.3$ .

### 3 Discussion

The analytical model of the O<sub>2</sub> distribution resulting from the EGEON model is a 7-parameters Chamberlain function of Europa centric distance  $R$ , angle from the subsolar point in the equatorial plane  $\alpha_{eq}$  and  $Lt$  as shown in eq (5). This model describes the O<sub>2</sub> profiles in the altitudes range from 1.05 to 5 R<sub>E</sub> according to the range of the source model P2013, nevertheless, the profiles could be extrapolated down to 1 R<sub>E</sub> as a first approximation. The EGEON model assumes non-collisional regimes. Possible close-to-surface additional effects are expected only at subsolar point where higher temperatures, up to 132 K, increase the H<sub>2</sub>O sublimation rate producing a vapor pressure of the order of 10<sup>12</sup> Pa, hence a non-collisional condition could occur (Smyth and Marconi, 2006; Plainaki et al., 2010). Only in that region the close-to-surface density profile could significantly differ from the extrapolated one.

The function trend versus altitude (parameters  $a$  of Eq. 1) is not  $\alpha$ -dependent or Configuration dependent at high altitudes. In fact, the density profile versus altitude is driven by the energy distribution of the emitted particles and at high altitudes only the more energetic particles released after radiolysis are present. The emitted O<sub>2</sub> energy distribution assumed in EGEON is a fit to an equivalent laboratory measurement (Johnson et al., 1982; Brown et al., 1984) used also in previous analyses:

$$dF / dE_e = a_n \times U_0 / (E_e + U_0)^2 \quad (7)$$

where  $U_0 = 0.015 eV$  (Shematovich et al., 2005),  $a_n$  is the normalization factor and  $E_e$  is the energy of the ejected O<sub>2</sub> molecules.

The parameters  $b$  and  $d$  are dependent on  $\alpha$ , as expected, since the released O<sub>2</sub> is dependent on the impacting ion flux and on yield of the release (number of particles released by single ion). The yield of the radiolytic release is dependent on temperature and on impacting energy (Famà et al., 2008).

The surface temperature map considered in P2013 was the one given in Spencer et al. (1999), based on Galileo mission data. In particular, the temperature map was assumed as  $40 + 50 \cos(Lt)^{1/4} + 40 \cos(\alpha)$  K in the dayside, and  $40 + 50 \cos(Lt)^{1/4}$  K in the nightside (Cassidy et al., 2007). A preferential O<sub>2</sub> ejection from the trailing hemisphere was considered in EGEON (see Eq. (4) in Plainaki et al. 2012). This may occur due to preferential ion (Pospieszalska and Johnson, 1989) or electron (Paranicas et al., 2001) irradiation. As evidenced in P2013 the temperature effect is predominant with respect to the impacting flux effect, but the release is higher when the trailing hemisphere coincides with the illuminated side, as well described by parameter  $p_2$ .

By fitting the vertical profile with the barometric profile, the exospheric temperature can be derived:  $\rho = \rho_1 \exp\left(-\frac{(R - R_1)}{H}\right)$ , where  $\rho_1$  is the density at  $R_1$  that is the

minimum altitude,  $H$  is the scale height defined as  $H = \frac{k_B T}{m_{O_2} \frac{GM_E}{R_1^2}}$ , where  $k_B$  is

the Boltzmann constant,  $m_{O_2}$  is the mass of a single molecule,  $G$  is the gravitational

constant,  $M_E$  is the Europa's mass. From these relations the temperature,  $T$ , can be easily derived.

As evidenced before, the obtained density profiles evidence that there are two exosphere scale heights, thus two temperatures describing the neutral population at low and high altitudes in the Europa's environment.

We performed two separate fits of the exosphere density profiles: one corresponding to region  $1.05 < R < 1.5 R_E$  (low altitudes) and one to region  $2 < R < 5 R_E$  (high altitudes). In Figure 12 the derived profiles at low and high altitudes are shown in the case of Conf *a* for the trailing and the leading hemisphere profiles.

It is clear that both the densities and the temperatures are higher in the illuminated side. The temperature at low altitudes in the illuminated side ( $T_{il}= 270$  K) is higher than in the dark side ( $T_{dl}= 210$  K), with a relative variation about 25%. This result can be interpreted as follows: the low-altitude  $O_2$  exosphere is the result of a density-weighted combination of both the surface-thermalized component (the surface temperature is about 130 K in the subsolar point) and the more energetic radiolytically-released population. The low temperature at low altitudes - dark side is the indication of a major weight of the population thermalized at lower temperatures, with respect to the illuminated side. The proposed scenario includes a first release after radiolysis with a yield proportional to ion flux and temperature, then the molecules start bouncing and to be thermalized with the surface. The lifetime of the thermalized component is driven by the loss via electron impact dissociation (considered symmetric and of the order of  $10^7$  s in the EGEON model), longer than the ballistic flight time (Plainaki et al. 2012), so that, the intense atmosphere around the moon is, in fact, generated by this thermalized population, as mentioned in the introduction.

The temperature for the higher altitudes is less variable, between 2170 and 2200 K; in fact, the relative variation is less than 2%. This uniformity was expected since the higher altitudes profile is generated by the temperature-independent energy distribution of radiolysis release (equation 7).

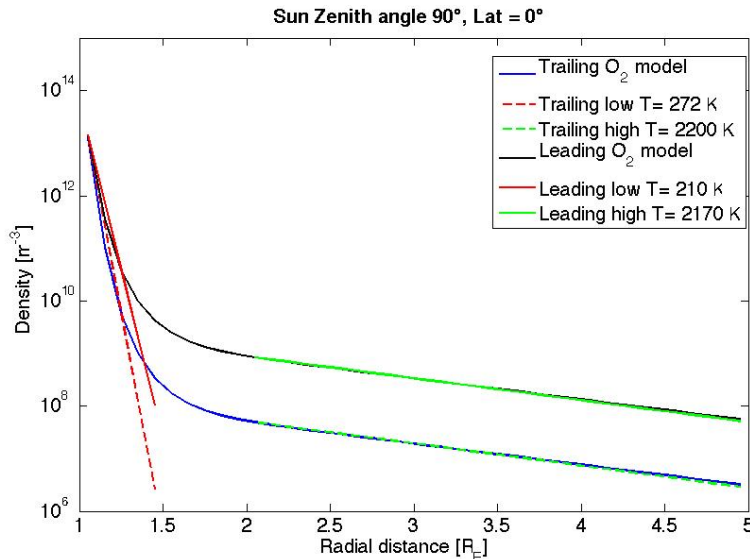


Figure 12 Examples of equatorial vertical profile for Conf *a* and derivation of temperature at low and high altitudes.

The two temperatures can be easily derived for each longitude and configuration (Figure 13).  $\Delta T_l/T_l$  is about 30% and  $\Delta T_h/T_h$  about 2%. The average scale height at low altitude is  $H_l= 0.03 R_E$  and at high altitudes is  $H_h=1.0 R_E$ . These quantities are

related to the parameters in Table 9. In fact, we can approximate the analytical model 6) at low altitudes as:

$$\rho_l (R < 1.5) \approx 10^{p2+p5} \exp\left(-\ln(10)\left(p5 p4 + \frac{1}{p1}\right)(R - 1)\right)$$

$$\rho_h (R > 2) \approx 10^{p2+p5 \exp(-p4)} \exp\left(-\ln(10)\left(\frac{1}{p1}\right)(R - 1)\right)$$

The analytical scale heights at  $R=1R_E$  and at  $R=2R_E$  are, then,  $H_l=0.014 R_E = 20$  km (corresponding to 124 K) and  $H_l=1.1 R_E = 1700$  km (2400 K), respectively, in agreement with the fitted-derived values.

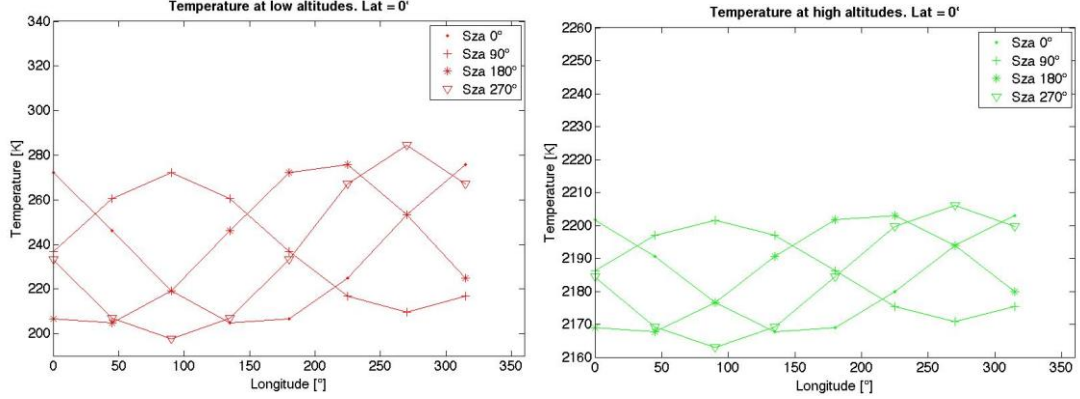


**Figure 13** Temperatures obtained at different longitudes for low (right) and high (left) altitudes for the four configurations.

We note that in the lower region ( $< 1.5 R_E$ ) the average scale heights estimated with our tool are in good agreement with the near-surface scale heights estimated in other studies. For example, Sittler et al. (2013), using the model by Amsif et al. (1997) and the parameters in Cassidy et al. (2007) estimated an  $O_2$  scale height that is increasing with altitude being equal to 20 km near the surface and 32 km at the altitude of about 600 km.

## 4 Conclusions

A 3D analytical model of Europa's  $O_2$  exosphere along the orbit around Jupiter (which finally provides the fourth dimension of the equation) has been obtained with a simple functional form described by equation (6). The final parameters of the total molecular oxygen density distribution are summarized in Table 10.

**Table 10** Analytical model parameters for total  $O_2$  density

Parameter	Functions
p1	2.51( $\pm 0.4$ )
p2	9.0-0.3* $\sin(\alpha_s)$
p3	0.71-0.09* $\sin(\alpha_s)$
p4	5.2
p5	5.825-0.045* $\sin(\alpha_s)$
p6	-0.92+0.155* $\sin(\alpha_s)$
p7	-28* $\cos(\alpha_s)$

As mentioned in the introduction, other molecular components like  $H_2$  and  $H_2O$  are expected to be the major exospheric constituents at high altitudes, nevertheless the  $O_2$

could be still a relevant fraction at higher distances. This model is intended to be the basic reference for the description of this O<sub>2</sub> component. In the future, we aim to develop further analytical models, with similar procedures, to describe also the other major components. This analytical model is a useful and user-friendly tool able to describe the bulk and especially the high altitude exospheric profiles and the expected asymmetries.

The model is able to reproduce the asymmetries in the O<sub>2</sub> distributions and their modulations due to the configurations among Europa, Jupiter and the Sun. Furthermore, the parameterization of the O<sub>2</sub> density distribution with parameters able to describe separately the different altitude ranges and the asymmetries in longitude and in orbit phase is an elegant way to quantify the density profile properties.

The analytical model permits to evidence and quantify the two-temperature components of the exosphere, and the longitude asymmetries of the low altitude temperatures.

This model could be optimized by including secondary effects like loss by dissociation by UV photons or charge-exchange with ambient plasma. It could be used as a tool in many possible applications in the context of a) theoretical studies related to the plasma-neutrals interactions at Europa; b) planning of either space mission observations or observations with ground and/or space telescopes; c) analysis of in situ and/or remote sensing data (e.g. obtained with HST and other telescopes). Here, we just highlight few examples.

- Through this tool, input for plasma circulation models can be provided and feedback for the evaluation of plasma sources (e.g. electron-impact ionization) and losses (e.g. charge-exchange) in the near-Europa space environment can be obtained
- During preparation for future missions to Europa, this tool can be used in ENA simulations; once future ENA measurements are available, the tool can be used while performing plasma deconvolution procedures.
- The tool can be used for the interpretation and analysis of the remote sensing observations, helping in the identification of sporadic phenomena.
- Through this tool the bulk exosphere population can be obtained; this information can be used as an input for minor exospheric species simulations.

The atmospheric physics of the Galilean moons of Jupiter, and in particular of Europa, is one of the major interests of the international scientific community. The recent observations with HST of Europa's O<sub>2</sub> environment (McGrath et al., 2004; Saur et al., 2011; Roth et al., 2014) and their potential implication on the nature of the moon's inner ocean, as well as subsequent debates on the interpretation of in situ and remote observations (Shemansky et al., 2014), opened a new chapter in the study of Europa's O<sub>2</sub> environment. In this context, the accurate characterization of the moon's exospheric O<sub>2</sub> background is a mandatory prerequisite. The analytical model presented in the current paper aims at providing the necessary link between observable quantities and physical processes. In particular, the scale heights for different components could be obtained during a mission to the icy moons. A comparison with the presently estimated quantities will directly provide information on the source process. Finally, the availability to the science community of the analytical model of Europa's O<sub>2</sub> exosphere may be of significant interest in view of the JUICE mission observations planning.

## **Acknowledgments**

Discussions in this paper have been partially performed in the context of the activities of the ISSI International Team #322, <http://www.issibern.ch/teams/exospherejuice/>. This work is partially supported by the ASI contract no. I/081/09/0.

## 5 References

Amsif 1997

- Boring, J.W., Garrett, J.W., Cummings, T.A., Johnson, R.E., Brown, W.L., 1984. Sputtering of solid SO<sub>2</sub>. *Nucl. Instrum. Methods B* 1, 321–326.
- Brown, W.L. et al., 1984. Electronic sputtering of low temperature molecular solids. *Nucl. Instrum. Methods Phys. Res. B* 1, 307–314.
- Cassidy, T.A., Johnson, R.E., McGrath, M.A., Wong, M.C., Cooper, J.F., 2007. The spatial morphology of Europa's near-surface O<sub>2</sub> atmosphere. *Icarus* 191, 755–764.
- Cassidy et al., 2010, Radiolysis and Photolysis of Icy Satellite Surfaces: Experiments and Theory, *Space Science Reviews*, 153, Issue 1-4, 299-315.
- Cassidy, T.A. et al., 2013. Magnetospheric ion sputtering and water ice grain size at Europa. *Planetary and Space Science* 77, 64–73.
- Chamberlain, J. W., 1963, Planetary coronae and atmospheric evaporation, *Planet. SpaceSci.*, 11, 901.
- Cooper et al., 2001, Energetic ion and electron irradiation of the icy Galilean Satellites, *Icarus* 149, 133-159.
- Famà et al. 2008, Sputtering of water ice by low energy ions, *Surface Sci.* 602, 156
- Johnson et al., 1982, Planetary applications of ion-induced erosion of condensed-gas frost, *Nucl. Instrum. Methods*, 198, 147
- Johnson, R.E., 1990. Energetic charged-particle interactions with atmospheres and surfaces. Springer-Verlag eds. ISBN 3-540-51908-4 Berlin Heidelberg New York
- Johnson et al., 2004. Radiation Effects on the Surface of the Galilean Satellites, in: *Jupiter-The Planet, Satellites and Magnetosphere*, Ed. F. Bagenal, T. Dowling, and W.B. McKinnon, Cambridge University, Cambridge. Chapter 20, 485-512
- Johnson, R.E., et al., 2009. Composition and Detection of Europa's Sputter-Induced Atmosphere. In: Pappalardo, R.T., McKinnon, W.B., Khurana, K.K. (Eds.), *Europa*. University of Arizona Press, Tucson.
- Leblanc, F., Johnson, R.E., Brown, M.E., 2002. Europa's sodium atmosphere: An ocean source? *Icarus* 159, 132–144.
- McGrath et al., 2004; Satellite atmospheres, In: *Jupiter. The planet, satellites and magnetosphere*. Ed. F. Bagenal, T. E. Dowling, W.B. McKinnon, Cambridge University Press., Vol. 1, 457 – 483
- Paranicas, C., Carlson, R.W., Johnson, R.E., 2001. Electron bombardment of Europa. *Geophysical Research Letters* 28, 673–676.
- Paranicas et al., 2002, The ion environment near Europa and its role in surface energetics, *Geophys. Res. Letters*, 29 (5), 1074
- Plainaki et al., 2010, Neutral particle release from Europa's surface, *Icarus*, 210, 385–395.
- Plainaki et al., 2012, The role of sputtering and radiolysis in the generation of Europa exosphere, *Icarus*, 218 (2), 956–966.
- P2013* Plainaki et al., 2013, Exospheric O<sub>2</sub> densities at Europa during different orbital phases, *Planetary and Space Science*, 88, 42-52.
- Plainaki, et al., 2015. The H<sub>2</sub>O and O<sub>2</sub> exospheres of Ganymede: the result of a complex interaction between the Jovian magnetospheric ions and the icy moon, *Icarus*, 245, 306–319.

- Pospieszalska, M.K., Johnson, R.E., 1989. Magnetospheric ion bombardment profiles of satellites—Europa and Dione. *Icarus* 78, 1–13.
- Roth et al. Transient water vapor at Europa's south pole. *Science*, 343, 171, 2014
- Saur, J. et al., 1998 Interaction of the Jovian magnetosphere with Europa: Constraints on the neutral atmosphere. *J. Geophys. Res.*, 103.
- Saur et al. 2011, Hubble Space Telescope/Advanced Camera for Surveys Observations of Europa's Atmospheric Ultraviolet Emission at Eastern Elongation, *Astroph. J.*, 738, 2, article id. 153.
- Shemansky, D. E. et al., 2014 Understanding of the Europa atmosphere and limits on geophysical activity. *Astroph. J.*, 797, 84.
- Shematovich et al., 2005, Surface-bounded atmosphere of Europa. *Icarus* 173, 480-498.
- Sittler 2013
- Smyth and Marconi, 2006. Europa's atmosphere, gas tori, and magnetospheric implications. *Icarus* 181, 510–526.
- Spencer et al. (1999)
- Wei et al., 2009. Influence of surface morphology on sputtering yields. *J. Phys. D: Appl. Phys.* 42 (2009) 165304 (6pp) doi:10.1088/0022-3727/42/16/165304